Mechanics of the Segmentation of an Embedded Fiber, Part I: Experimental Investigations

A. ten Busschen
Laboratory of Engineering Mechanics, and Marine Technology, Delft University of Technology, Delft, The Netherlands

A. P. S. Selvadurai
Department of Civil Engineering and Applied Mechanics, Faculty of Engineering, McGill University, Montreal, QC H3A 2K6, Canada
Mem. ASME

Micromechanical modeling is an important aspect in the study of fiber-reinforced composites. In such studies, an important class of structural parameters is formed by the interaction between the matrix and the embedded fibers. These interactive processes can be investigated by an appeal to a test which involves the segmentation of an embedded fiber. This test is referred to as a "fragmentation test." During a fragmentation test, two distinct fracture phenomena are observed. These phenomena are directly related to the integrity of bond between the embedded fiber and the matrix. The first phenomenon involves situations where the interface bond is weaker than the matrix material. In this case the fiber fragment ends will slip and in this region shear stresses are transmitted by friction and/or interlocking mechanical actions. In contrast, when the interface bond has stronger properties than the matrix material, cracking will occur in the matrix region. Here, a crack initiated in the fiber will propagate into the matrix region typically forming conoidal cracks, or combinations of conoidal and flat cracks. This paper describes the background of the fragmentation test and the associated experimental research. Attention is focused on the experimental evaluation of matrix fracture topographies encountered in the fragmentation test.

Introduction

Composite materials offer new possibilities for the design of engineering structures. A majority of modern advanced composite materials is formed by fiber-reinforced plastics which can combine low specific weights with high strength. A critical engineering property of such composites is the transverse strength, i.e., the strength normal to the aligned fibers. The wide variations in the transverse strength property places a severe restriction on the wider applications of fiber-reinforced plastics (see, e.g., Hull, 1981; Pagano, 1989; Friedrich, 1989; Kedward et al., 1989; Pantano and Chen, 1990; ten Busschen, 1991). By gaining insight into the mechanisms that are responsible for the magnitude of transverse strength, it is possible to identify techniques and properties which could lead to improvements in the transverse strength characteristics. Micromechanical modeling provides a basis for the prediction of macroscopic mechanical properties of a composite, based on the so-called structural parameters. Thus, relationships can be obtained between the properties at the microscale (structural parameters) and macroscopic composite behavior (effective behavior). This is an effective basis for the identification of the parameters which contribute to low transverse strengths in composites (ten Busschen, 1991).

The structural parameters needed for micromechanical modeling can be divided into three groups; the first group consists of the properties of the constituents of the composite (i.e., matrix, fibers); the second group is formed by the properties of the interaction between the constituents (i.e., interfaces, delaminations); the third group is formed by the morphology of the reinforcement (i.e., fiber content, fiber distribution, and arrangement). In the second group of structural parameters, the interaction between the constituents, or more specifically the mechanical contact between the fiber and the matrix is known to affect the mechanical properties of the composite, and especially the transverse strength (Moran et al., 1991). A variety of tests can be developed to characterize the mechanical response of the contact between a fiber and the surrounding matrix; these include, for example, the single fiber pull-out test and fragmentation test involving a single filament composite specimen.

The composites research program at the Laboratory of Engineering Mechanics at Delft University of Technology has initiated a series of experimental investigations geared to the evaluation of the mechanical characteristics of a fiber-matrix interface by appeal to the fragmentation test (van den Berg, 1990). The fragmentation test uses a specimen that consists of a single fiber filament which is embedded in a polymer matrix specimen (Fig. 1). Upon application of a

Contributed by the Applied Mechanics Division of The American Society of Mechanical Engineers for publication in the ASME Journal of Applied Mechanics.

Discussion on this paper should be addressed to the Technical Editor, Processor Lewis T. Wheeler, Department of Mechanical Engineering, University of Houston, Houston, TX 77204-4792, and will be accepted until four months after final publication of the paper itself in the ASME Journal of Applied Mechanics.

Manuscript received by the ASME Applied Mechanics Division, Dec. 2, 1992; final revision, Oct. 8, 1993. Associate Technical Editor: G. J. Dvorak.

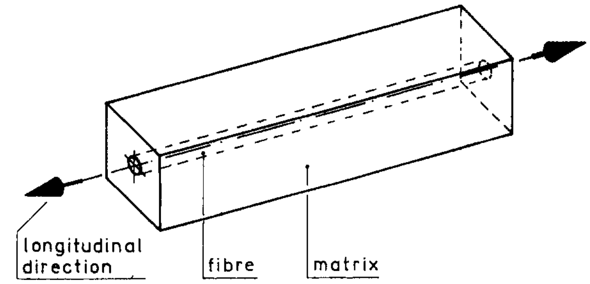

Fig. 1 Configuration of test specimen with embedded fiber

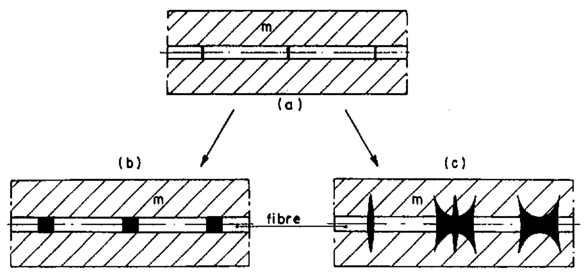

Fig. 2 Observed damage phenomena during fragmentation tests (*a*) cracked fiber, (*b*) formation of voids (weak interface), (*c*) matrix crack formation (strong interface)

longitudinal strain to the specimen, the intact fiber will also be subjected to an identical strain. When the longitudinal strain reaches a certain magnitude, the fiber will experience fracture at several locations (Fig. 2(*a*)). If the strain is increased further, two distinct phenomena can be observed. These phenomena are directly related to the adhesive properties of the fiber-matrix interface. When the strength or fracture properties of the mechanical contact are weaker than those of the matrix, the fiber fragment ends will move relative to the specimen (slip), forming an increasing void with increasing strain (Fig. 2(*b*)). In contrast, when the interface strength and fracture properties are stronger than those of the matrix material, the fiber crack will extend into the matrix region (Fig. 2(*c*)). The occurrence of both phenomena at prolonged fragmentation was reported by Selvadurai et al. (1991). The occurrence of either slip at the interface or cracks in the matrix is directly influenced by the integrity of the interface. Consequently, identical fiber-matrix systems will display radically different post fiber-fracture processes depending upon the coupling agents that are utilized to enhance the interface fracture and failure characteristics.

This paper forms the first part of a study which investigates the mechanics of a fragmentation test. It discusses the experimental investigations which were carried out at the Laboratory of Engineering Mechanics at Delft University of Technology. The mechanical background of the fragmentation test and the test procedure are described. Special attention is given to the techniques used in the measurement of strains in the specimen and the characterization of fine matrix microcracks which occur at the cracked fiber locations. An image analysis technique forms the basis for such experimental evaluations. The experimental results are presented and the characteristic features of "Bat Cracks" are quantified. A companion paper will focus on the computational modeling of the process of matrix crack extension at cracked fiber locations.

Mechanics of the Fragmentation Test

Fiber Reinforcement. Most reinforcing fibers employed in advanced composite materials are composed of brittle elastic materials. Typical examples of such materials include carbon fibers, graphite fibers, boron fibers, silicon carbide fibers and E-Glass. In this article attention is focused on the class of fiber-reinforced composites composed of E-Glass fibers. These brittle materials generally have an extremely high intrinsic strength (theoretical strength); however, in practice, the actual strength of such materials is strongly influenced by the geometrical imperfections. This can be attributed to processes such as notch, surface flaw, or internal flaw sensitivity which can drastically reduce the measured strength (see, for example, the classical study by Griffith, (1921). For this reason, fibers for composite reinforcement are manufactured as thin as possible; this reduces the probability of occurrence of strength-reducing flaws. From these observations it becomes evident that the effective strength of a reinforcing fiber is dependent on the fiber length; i.e., it increases with decreasing length (see, e.g., Merle and Xie, 1991). Although long fibers used in composites do contain many flaws, it is assumed there are no disadvantageous effects in the generation of longitudinal strength in a composite due to the load transfer mechanisms that occur within the matrix phase.

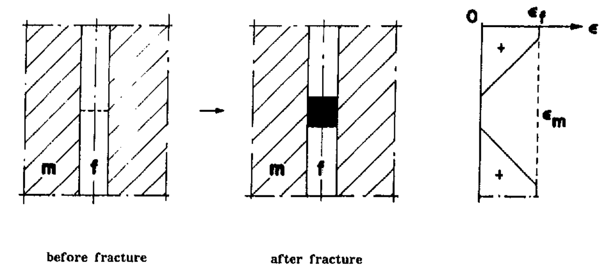

Fig. 3 Formation of a void at a cracked fiber

The Fragmentation Test. The fragmentation test consists of the straining of a matrix specimen which contains a co-axial single fiber (or single filament). The dimensions of the single fiber, relative to the dimension of the matrix region are such that, effectively, the fiber is embedded in a matrix region of infinite extent (i.e., $d/t = 0.015$; where $d = 15\mu$m; $t = 1$ mm and t is the thickness of the specimen). The fragmentation test specimen is subjected to uniform strain over its entire cross-section. When the strain reaches a certain value, the fiber will fracture at its weakest locations. If the strength and fracture characteristics of the fiber-matrix interface are lower than those of the matrix material, interface slipping and/or interface locking can occur at a detached interface. This phenomenon can be explained by the unloading of cracked fiber ends after fracture. In this instance the fiber strain will be zero at the cracked ends and by gradual load transfer processes the longitudinal strains in the fiber will reach the same magnitude as the matrix strain. Over the distance where gradual load transfer takes place the incompatibility of strains between the matrix and the fiber usually results in the formation of a void (Fig. 3).

In Fig. 3, the fiber strain is assumed to be linear in the longitudinal direction over this slipped section. It is often assumed that the shear stresses in the interface region where slipping takes place has constant value (see, e.g., Piggot, 1980). This constant shear stress is regarded as a strength property of the interface (i), indicated by τ_i. To account for the difference in fiber strain and the matrix strain, the matrix exhibits shear deformation besides slip at the fiber-matrix interface. Such mechanisms can be described by shear-lag theory (Cox, 1952) and by more advanced load transfer models (McCartney, 1989). However, the effects of shear deformation of the matrix material is negligible when compared to the effect of slipping of the interface (van den Berg, 1990).

Critical Fiber Length. With the assumption that the shear stress is constant in the parts of the fiber-matrix interface where slip occurs (slip theory), attention can be focused on a fiber fragment between two fractures with slip regions (S) at the ends (Fig. 4). By means of the shear stresses at the fragment ends, the fiber can be loaded in the middle part (M) until the fiber strength is reached again forming a new fracture in the fiber, etc. A critical situation occurs when the middle part disappears (slip over the entire fragment). In this case the largest possible loading of the fiber occurs, which gives the maximum fiber stress in the middle of the fiber fragment, indicated by $\sigma_{f,\max}$:

$$\sigma_{f,\max} = \frac{2l\tau_i}{d_f}. \tag{1}$$

In this connection, the critical fiber length is defined as the length at which the maximum fiber stress in (1) equals the fiber strength indicated by $\langle \sigma_f \rangle$ (belonging to a particular fiber length) i.e.,

$$l_{cr} = \frac{d_f \langle \sigma_f \rangle}{2\tau_i}. \tag{2}$$

This critical fiber length is the shortest fiber fragment that can fracture under the given assumptions. In the case of fiber slip, the fragmentation test is terminated when further straining of the specimen does not cause new fractures in the fiber fragments; in this case all the fragments will not be longer than the critical length (assuming the validity of the slip theory). When the fiber diameter and fiber strength (at critical length) are known the average fragment length indicated by l can be used to determine the slip length of the interface, e.g.,

$$\tau_i = \frac{d_f \langle \sigma_f \rangle}{3l}. \tag{3}$$

The above result is based on the fact that fiber fragments with critical length have equal probability either to fracture or not to fracture. In this case of fracture the resulting separate parts have to be accounted for in the calculations. With this simple model, the mean fragment length can be expressed in terms of the critical length: i.e.,

$$l = \frac{2}{3} l_{cr} \tag{4}$$

The result (4) which was also reported by Merle and Xie (1991) can also be derived by employing a more sophisticated simulation where the fragment lengths are not required to assume the critical length or half of the critical length.

Formation of Cracks. If the strength and fracture toughness of the interface are higher than those of the matrix material, the ends of the cracked fiber will remain adhered to the matrix thus forcing the crack to extend into the matrix. The explanation and evaluation of the mechanical aspects of this crack growth will be given in the ensuing sections.

Let us first consider the case of the classical penny-shaped crack which is located in an elastic matrix of infinite extent and subjected to a uniform stress field at infinity (σ_∞) (see, e.g., Fig. 5). The Mode I stress intensity factor at the crack tip can be obtained from the classical result given by Sneddon (1946) (see also Kassir and Sih, 1975), i.e.,

$$K_I^0 = \frac{2\sigma_\infty \sqrt{c}}{\pi} \tag{5}$$

where c is the radius of the penny-shaped crack. For a polyester matrix it is possible to determine the extent of cracking necessary prior to reaching the strength of the matrix material σ_{mt}. The limiting case occurs when the remote stress σ_∞ reaches the material strength at the same instance when the stress intensity factor reaches its critical value K_{Ic}, i.e.,

$$K_{Ic} = \frac{2\sigma_{mt}\sqrt{c}}{\pi}. \tag{6}$$

Thus for crack extension prior to reaching the material strength, the minimum crack radius required is given by

$$c_{\min} = \left(\frac{\pi K_{Ic}}{2\sigma_{mt}}\right)^2 \tag{7}$$

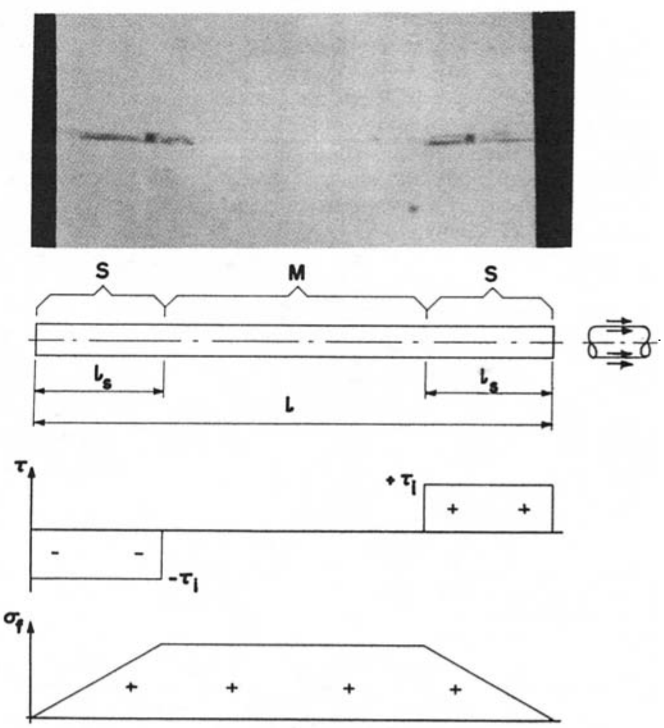

Fig. 4 Fiber fragment with slipping end; observed phenomena and modeling

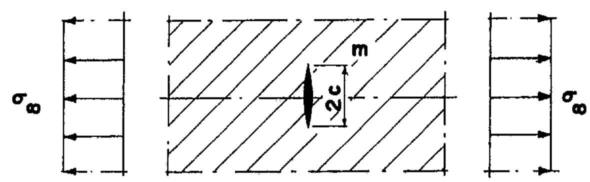

Fig. 5 Penny-shaped crack in an elastic medium of infinite extent

Table 1 Minimum crack radii for a polyester matrix

Curing state	K_{Ic} (MPa $\sqrt{m}$) Rebelo et al. (1986)	σ_{mt} (MPa) Berg (1990)	$c_{\min}$ (μm) From Eq.(7)
seven days after solidification	1.0	53	846
after post-cure treatment	0.6	87	117

The Table 1 gives results for $c_{\min}$ for polyester matrices at various stages of the hardening phase. From Table 1 it can be concluded that pre-existing penny-shaped cracks have to be several times the size of the fiber diameter (15 μm) to permit crack propagation. It should be noted that polyester shows the lowest critical Mode I stress intensity factor and the highest material strength after a full post-cure treatment. This hardening state, therefore, yields the lower bound for the minimum crack radius.

Let us now focus attention on the case of the *fiber matrix crack* in which a penny-shaped crack extends through a cracked fiber into the matrix region (Fig. 6). This problem was investigated by Selvadurai (1991) by using a boundary element modeling of the fracture mechanics problem. More recently Selvadurai et al. (1995) have also developed a complete analytical solution for the integral equations governing the mixed boundary value problem. In the case of the fiber-matrix crack, the Mode I stress intensity factor is significantly higher than that for the penny-shaped crack. For typical fiber-matrix cracks (Fig. 6), the stress intensity factors are given as a function of the modulus mismatch between the fiber and the matrix (Fig. 7). From these results it may be concluded that in situations where the interface strength and fracture toughness are sufficient enough to prevent slip processes, the fiber crack will propagate into the matrix. With stiffer fibers (i.e., $E_f/E_m > 1$) the stress intensity factor at the matrix-fiber crack tip is sufficiently amplified to cause crack propagation prior to reaching the matrix strength. Although a penny-shaped crack is intuitively thought to be the most likely crack propagation mode subsequent to fiber fracture, other crack topographies are possible depending upon local inhomogeneities and the degree of localized damage that can be induced in the matrix region at the location of a cracked fiber (Selvadurai et al., 1991). Figure 8 illustrates four crack topographies that were observed in the fragmentation tests involving an E-Glass Fiber embedded in a polyester matrix. Other researchers have also observed similar crack patterns in materials with stiff inclusions. For example, penny-shaped cracks and conoidal cracks were observed in Boron fiber-Epoxy systems (Chamis, 1974) and glass bead-polystyrene composite systems (Dekkers, 1985). Similar crack patterns in fragmentation tests with carbon fiber-epoxy systems were reported by Sancaktar (1991). The main categories of crack patterns observed in actual fragmentation tests are shown in Fig. 9. These fracture patterns are characterized by the fiber crack separation distance $2u_0$, the diameter of penny-shaped cracks $2c$, the crack termination diameter of purely conoidal crack ($2c$), the crack termination diameters for combined cracks involving penny-shaped ($2c_2$) and conoidal cracks ($2c_1$) and the inclination of the conoidal crack to the axis of the fiber (θ_0). In general

$$\left\{\frac{u_0}{a}, \frac{c}{a}, \frac{c_1}{a}, \frac{c_2}{a}\right\} = f\left\{\frac{E_f}{E_m}, \nu_f, \nu_m, K_{Ic}, K_{IIc}, \epsilon_\infty\right\} \quad (8)$$

where $\epsilon_\infty \simeq \sigma_\infty/E_m$.

In connection with the crack inclination θ_0, the following observations can be made. First, in the experiments, this angle can have different values; in any calculation (Selvadurai and ten Busschen, 1995) this parameter needs to be assigned a specific value in order to examine the progress of matrix crack extension at a cracked fiber location. Secondly, consider the local geometry in the vicinity of a cracked fiber location. Referring to Fig. 10, two possible scenarios exist. In the first case strong interface bond will propagate the elemental or starter matrix cracks (e.g., penny-shaped and conical) into the matrix region. With weaker interface bond, delaminations can occur along the interface ($\theta_0 = 0$ deg). As can be observed in Fig. 10, the locations A correspond to points which are located at bi-material interface regions. Consequently, oscillatory stress singularities will be observed at the locations A. The stress singularities K_I and K_{II} at such crack extremities will exhibit an oscillatory character (see, e.g., Williams, 1959; England, 1965; Sih and Chen, 1980;

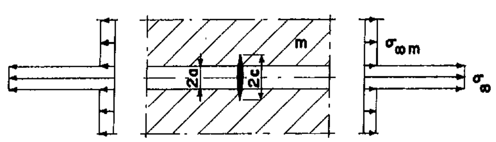

Fig. 6 The matrix-fiber crack in an elastic medium of infinite extent

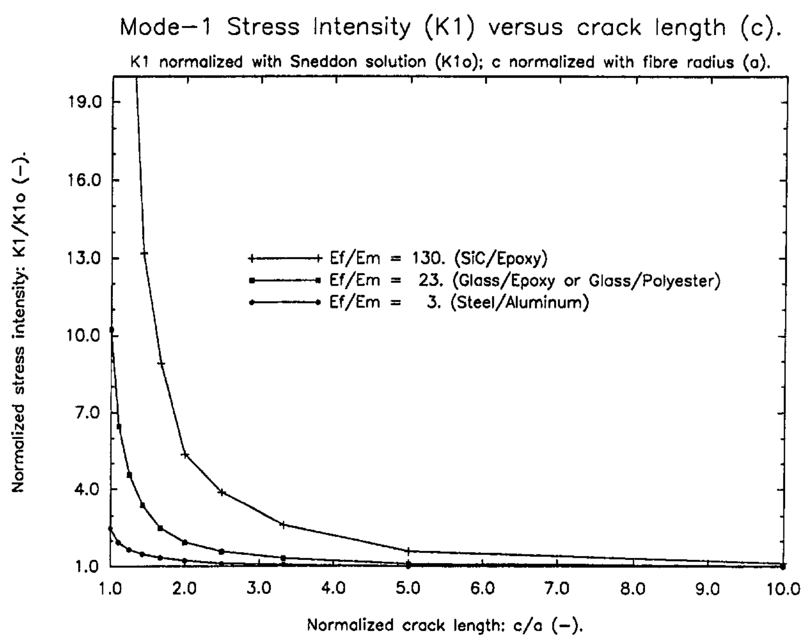

Fig. 7 The stress intensity factor for the penny-shaped matrix-fiber crack: influence of fiber-matrix mismatch, K_1 = stress intensity factor for the penny-shaped matrix fiber crack, K_0 = stress intensity factor for the penny-shaped crack in a matrix region

Atkinson, 1979). In the case of the matrix crack (locations B in Fig. 10) the stress intensity factors will either be purely K_I or K_I and K_{II}, depending upon the crack type. When the stress intensity factors at the fiber-matrix interface at the location A are lower than the associated critical values and when the stress intensity factors at the matrix location B reach their critical values, the crack will propagate into the matrix.

Experimental Procedure

Materials. The fibers used in the experiments were supplied by PPG Industries Fiber Glass bv. The commercially available fibers contain a sizing; however, the fibers used in the current series of tests were especially prepared by PPG Industries Fiber Glass bv and contained only a coupling agent (Gamma-glycid-oxypropyl-trimethoxy-silaan, A-187). For the matrix material, an isophtalic-based unsaturated Polyester was used; Synolite 593-A-2 (see, e.g., DSM Resins, 1991). The choice for these materials is based on prior experience with these materials which enables the use of results derived from other experimental investigations to supplement the required material characteristics (ten Busschen, 1991).

Manufacture of Specimens. In order to cast single filaments in the polyester matrix a special mould is constructed. The co-axial alignment of the fiber of filament within the test specimen is an important requirement of the specimen fabrication process. In order to maintain the filaments straight, they are subjected to a nominal tension by the application of static weights (Fig. 11). The application of the tension is also necessary to prevent the filaments from touching the sides of the mould. Due to the exothermic reaction during solidification, the thicker regions of the cast (these locations are indicated by a star (*) in the mould illustrated in Fig. 11) will first start to become a solid. Thus the middle part that is still liquid (located at the removable part) will be insulated during solidification between blocks of matrix material that have already solidified. Unfortunately, polyester exhibits volume shrinkage during solidification, which results in "lake formation" at the surfaces of this captured midsection. The remedy to alleviate this problem was to install a removable part in the mould that can follow the shrinkage of the middle part of the cast (see Fig. 11). During solidification, the bolts of the removable parts are released so that these parts can follow the shrinkage. After completion of solidification, the cast is released from the mould and sawed into specimens, using a

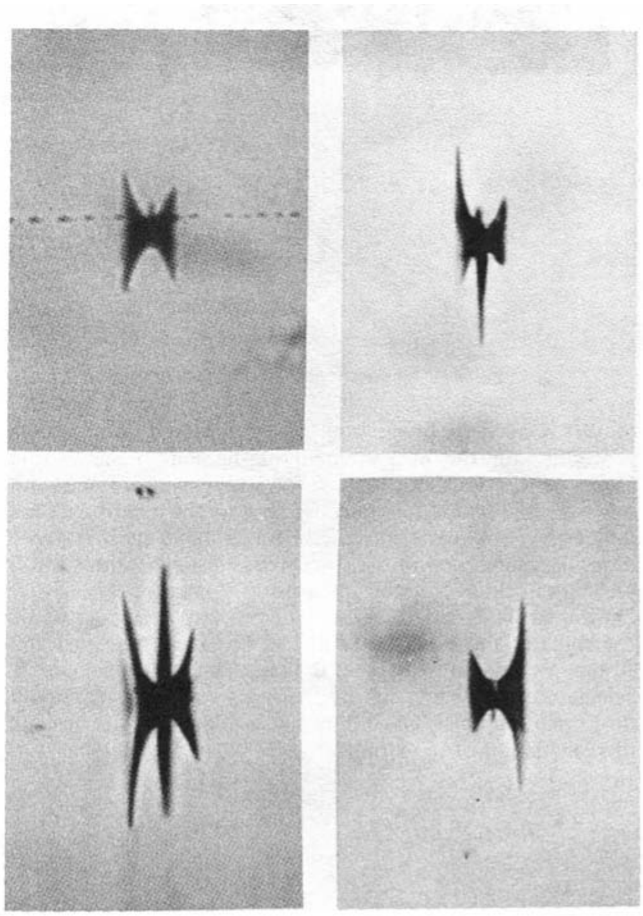

Fig. 8 Photographs of observed cracks during a fragmentation test

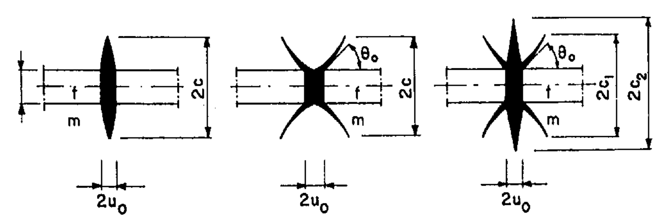

Fig. 9 Main crack extension geometries

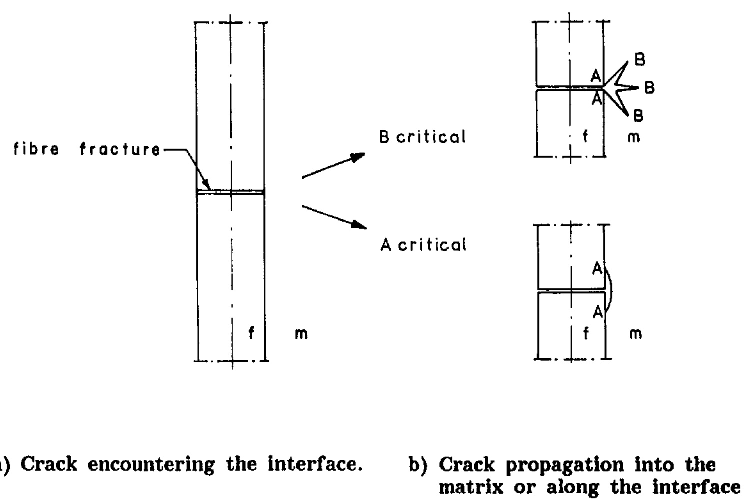

Fig. 10 Matrix and interface crack configurations at a cracked fiber location

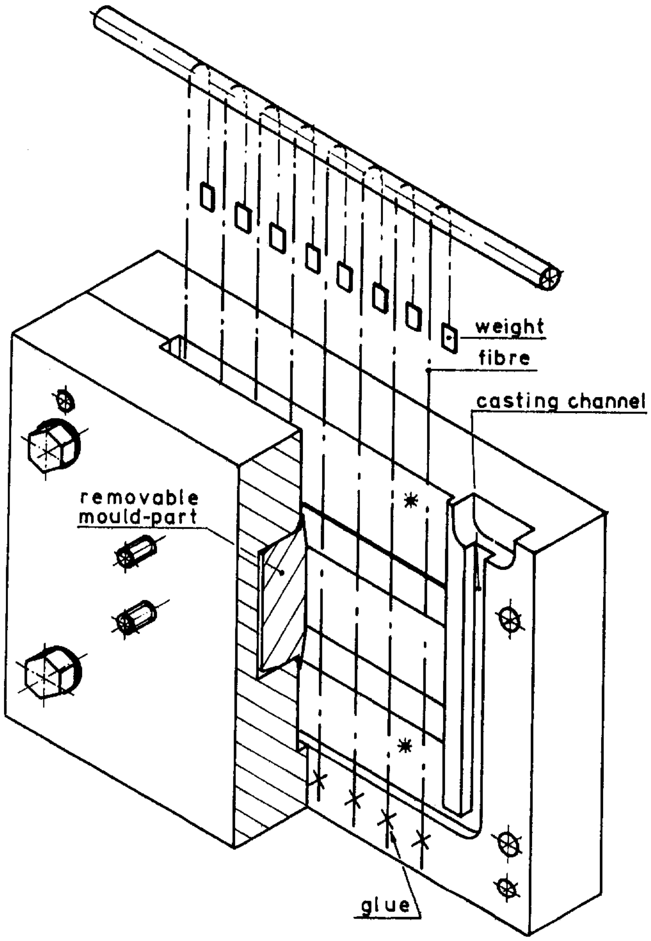

Fig. 11 Fiber filament assembly in casting location

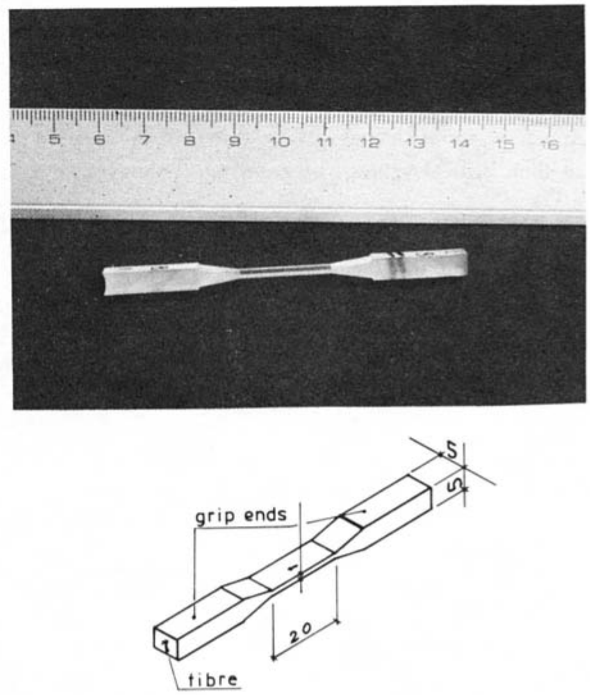

Fig. 12 The fragmentation test specimen

diamond saw. The shape and dimensions of the final specimen are shown in Fig. 12. The precise dimensions of the middle section of the specimen are carefully measured for each specimen in order to accurately define the matrix stress in this region during testing. The test is carried out seven days after solidification (the specimens are kept at 23°C at 50 percent relative humidity).

Testing. The specimens are tested in a servo-controlled tensile testing machine, which applies a constant displacement rate at the free grip end. The rate corresponds to

$$\dot{u}_{\text{grip}} = 0.40 \text{ mm/min}.$$

Initially the specimen exhibits linear elastic response and the strain rate in the midsection ($d\epsilon_{zz}^o/dt$) can be approximated by the result

$$\frac{d\epsilon_{zz}^o}{dt} = \dot{\epsilon}_{zz}^o \simeq \frac{\dot{u}_{\text{grip}}}{20} = 0.02\ (\text{min})^{-1} = 2 \text{ percent } (\text{min})^{-1} \tag{9}$$

(It should be noted that the components of the overall strain of the specimen (ϵ_{ij}^o) are macroscopic or homogenized components, as opposed to the components of the strains in the specimen (ϵ_{ij}), which are microscopic components. The z-axis is defined to be the fiber direction and the y-z plane is defined to be the plane in which the strains are measured).

At relatively high stress levels, (stresses approaching the tensile strength σ_T of the polyester = 87 MPa), the polyester behavior exhibits a nonlinear response. Furthermore, a more accurate approximation of the strain in the middle section (than those that can be derived from the strain rate defined by (9)) is needed. Image analysis is identified as a suitable procedure for the measurement of the longitudinal strain. Other conventional techniques for strain measurement cannot be adopted for this purpose due to the relatively small dimensions of the test specimen. In the image analysis procedure, the midsection of the specimen is installed with sprayed or marker dots of paint measuring approximately 20μm. During straining of the specimen, the displacements of the centroids of these marker dots are observed. The principal strains associated with the in-plane deformations can be calculated by utilizing the displacements of the centroids of three marker dots. The following relationships are used in the calculation of the strains:

$$\begin{aligned}
\Delta y_{021} &= y_{02} - y_{01} \quad ; \quad \Delta u_{y21} = u_{y2} - u_{y1} \\
\Delta z_{021} &= z_{02} - z_{01} \quad ; \quad \Delta u_{z21} = u_{z2} - u_{z1} \\
\Delta y_{031} &= y_{03} - y_{01} \quad ; \quad \Delta u_{y31} = u_{y3} - u_{y1} \\
\Delta z_{031} &= z_{03} - z_{01} \quad ; \quad \Delta u_{z31} = u_{z3} - u_{z1}
\end{aligned} \tag{10}$$

in which y_{0i} and z_{0i} are coordinates of point i in the undeformed state. Provided the macroscopic strain field is homogeneous and the displacement gradients are small, the displacement field for the kth load step can be obtained from the relationships

$$\begin{bmatrix} \Delta u_{y21} \\ \Delta u_{z21} \\ \Delta u_{y31} \\ \Delta u_{z31} \end{bmatrix}_k = \begin{bmatrix} \Delta y_{021} & \Delta z_{021} & 0 & 0 \\ 0 & 0 & \Delta y_{021} & \Delta z_{021} \\ \Delta y_{031} & \Delta z_{031} & 0 & 0 \\ 0 & 0 & \Delta y_{031} & \Delta z_{031} \end{bmatrix} \times \begin{bmatrix} \partial u_y/\partial y \\ \partial u_y/\partial z \\ \partial u_z/\partial y \\ \partial u_z/\partial z \end{bmatrix}_k . \tag{11}$$

This result can be written in the compact form

$$[\Delta \mathbf{u}]_k = [\Delta \mathbf{r}_0] \left[\frac{\partial \mathbf{u}}{\partial \mathbf{r}} \right]_k . \tag{12}$$

The vector of displacement gradients $[\partial \mathbf{u}/\partial \mathbf{r}]_k$ can be determined from the initial relative positions of the centroids, $[\Delta \mathbf{r}_0]$, and the relative displacements of the centroids $[\Delta \mathbf{u}]_k$ by inversion of the result (12), i.e.,

$$\left[\frac{\partial \mathbf{u}}{\partial \mathbf{r}}\right]_k = [\Delta \mathbf{r}_0]^{-1}[\Delta \mathbf{u}]_k. \tag{13}$$

The strain in the specimen along the direction of loading (ϵ_{zz}^o) and perpendicular to this direction (ϵ_{yy}^o) can be calculated from the results

$$\epsilon_{zz}^o = \frac{\partial u_z}{\partial z}; \quad \epsilon_{yy}^o = \frac{\partial u_y}{\partial y} \tag{14}$$

During an experiment, the camera is accurately positioned with its horizon parallel to the axis of the specimen. The maximum misalignment in this configuration is found to be 0.01 radians, so that the difference between the strains that can be calculated in (14) and the principal strains in the $y-z$ plane of the specimen will be negligible. Using the Image Analysis System, the strain field in a stressed specimen could be determined to within an accuracy of $2\,\mu$m/mm (= 0.2 percent strain). It is also noted that the initial elastic properties of the matrix material can be estimated by using the results for the applied load and the resulting strain. This procedure was carried out by optimizing five sampling points that were determined when the specimen strain was between 0.5 percent and 1.0 to be representative of the range of strain for initial elastic behavior of the matrix material. The results associated with this procedure is shown in Table 2. The results indicate a large variation in the value of E_m which can be attributed to the incomplete curing of the polyester matrix. The representative value of $E_m \simeq 1500$ MPa is consistent with results derived from other investigations (Busschen, 1991). Testing is terminated after the fragmentation process is saturated (i.e., no new fragments are observed during further straining). After a test, the cracks are investigated with the Image Analysis System, using the TCL-Programme (Toussaint, 1991) for processing the images. The complete procedure for analyzing the images of the matrix cracks is described in the ensuing section.

Experimental Results

Data Evaluation. After a fragmentation test, each specimen contains about 50 cracks. A large proportion of these cracks can be classified according to the three main crack geometries illustrated in Fig. 8. Other cracks can have helicoidal shapes (see, e.g., Fig. 13). These cracks, however, will not be taken into consideration in the data reduction process. The cracks to be evaluated will be subjected to the ensuing procedure for purposes of comparison with numerical simulations. The image of the crack is first recorded using a microscope (Type Panphot 407650, Ernst Leitz GmbH) with a magnification of either 165x, 225x, or 450x (depending on the dimensions of the cracks, the measurements will be scaled to the fiber radius) and a digital camera (type CCD video camera 91750155 Sanyo). With the digital camera a picture is recorded, containing 256×256 pixels in which each pixel has grey-value that may range from 0 (black) to 255 (white). The 386, 25 MHz computer (with math coprocessor) in which these images are recorded also contains the TCL-Programme (Toussaint, 1991). After the image of the crack is stored, the contrast is stretched; i.e., the range of grey-values of the actual image (which usually does not cover the range from 0 to 255) is stretched from 0 (black) to 255 (white). The effect of this stretching process is illustrated in Fig. 14.

After this procedure a threshold value of grey-values is chosen. Pixels with a grey value below this value are considered to be a part of the crack and are made black; other pixels are considered to be outside of the crack and are made white. Thus a binary image is obtained. The choice for a threshold value is made by taking the largest value that is possible provided that (i) discrepancies that do not belong to the crack (shadows, etc.) are not connected to the upper or

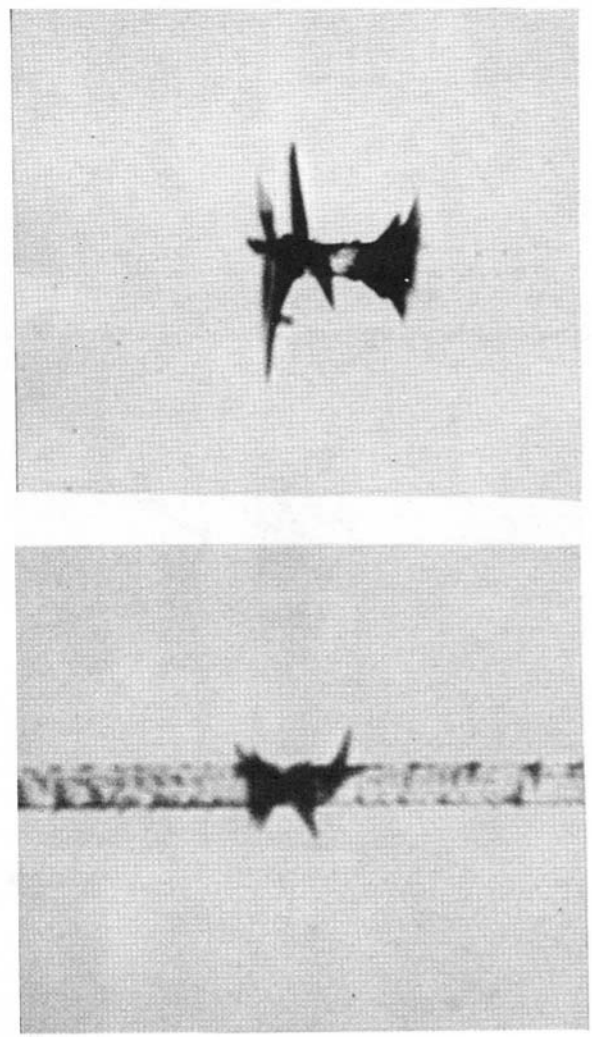

Fig. 13 Helicoidal matrix cracks

Table 2 Measured data for test specimen

Specimen	Maximum strain $\epsilon_{zz,\max}^o$ (%)	Initial stiffness E_m (MPa)	Initial Poisson's Ratio ν_m (-)
1	4.3	1550	0.35
2	7.7	2060	0.33
3	8.6	2190	0.35
4	8.8	1080	0.40
5	10.8	1390	0.26

lower part of the crack and (ii) the disturbances themselves do not have an area larger than the crack area. In Fig. 15, this is illustrated with three threshold values, employed on the same crack. With the high threshold value, disturbances around the crack are assigned to the crack region; the middle value shows disturbances that are unconnected to the crack; the low value shows a crack that has smaller dimensions than in the case of the midvalue.

The binary image that is obtained after the threshold procedure of contour of the image is determined with the TCL Programme (Fig. 16). Of this contour only the upper part and the lower part are needed to determine parameters necessary for comparison with numerical simulations. From the contour lines, the skeletal lines or crack outlines are determined (Fig. 17(*a*)). The end points of the skeleton lines are used for the y-coordinate of the position of a box region employed to remove tips of conical cracks (Fig. 17(*b*)). This procedure is adopted to remove from the crack tip the following: the side contour of the entire crack and the strongly curved part of the tips of the conical cracks. Also, the tip of the penny-shaped crack is used to determine the location of y-axis; in the conical case, the point with the lowest absolute value of y in the upper or lower contours is used for this purpose. Thus the upper and lower contours of the crack under consideration are determined (Fig. 18).

The upper and lower contours are rastered in order to define discrete points in pixel coordinates. The fiber location is indicated manually by specifying four separate points corresponding to fiber edges around the crack. If only three fiber edges are visible, the fiber radius and the middle of the fiber are determined by an iterative procedure. In this case the crack image under consideration is classified as *accurate*. If this is not possible (due to the fact that two or more of the fiber edges are not visible), the edges are indicated as accurately as permissible and the crack image under consideration is classified as *approximate*. The results of these two

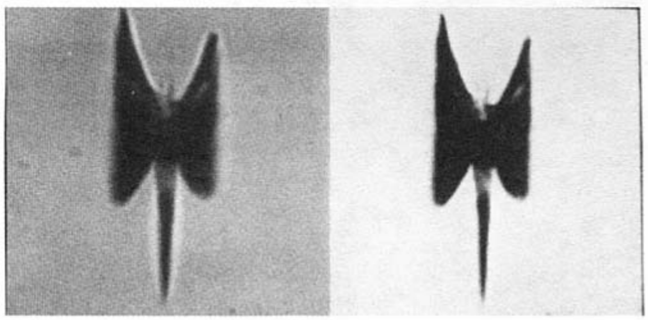

Fig. 14 Effect of stretching of grey-values on definition of crack outline

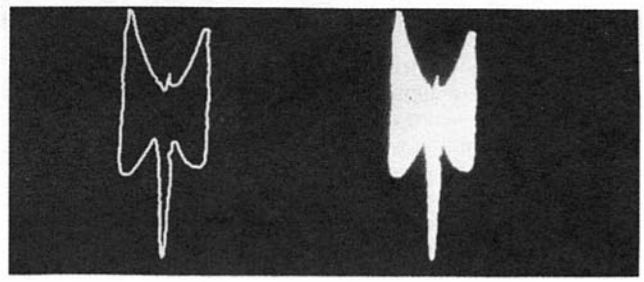

Fig. 16 Contour of the binary image of matrix crack

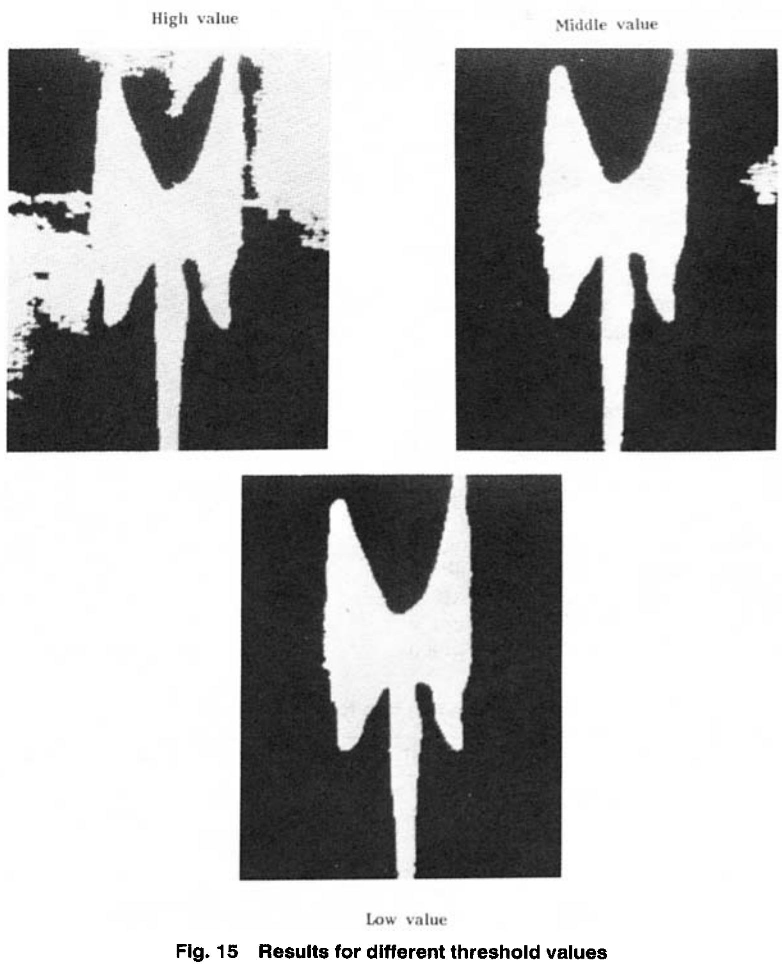

Fig. 15 Results for different threshold values

classes of crack images will be treated separately. The fiber edges that are indicated (either *accurate* or *approximate*) will determine the location of the z-axis (the direction of the z-axis is taken as the same as the horizontal of the image of the camera). Furthermore, the fiber radius (required for nondimensional plots) is also confirmed by this procedure. All the contour halves of the cracks are made dimensionless with respect to the fiber radius (a). For each class of contour halves, the results are superimposed. Examples of such grouped results are shown in Fig. 19. For each class of contour halves and for each specimen, an average contour is determined by means of a path searching technique procedure available in the TCL software. Also, an optimum path is determined by considering all contour halves.

The contour halves determined via the above procedure are used to determine the values of c/a, c_1/a, c_2/a, and θ_0. The crack images do not possess the degree of refinement which enable the determination of u_0/a. The crack topographies generally obstruct the visibility of the cracked fiber.

Fracture Geometries

In this section, the results determined from five specimens are presented. These specimens have different levels of strain at which the fragmentation test is terminated. Furthermore, for every specimen, the initial elastic properties of the matrix are calculated for purposes of comparison. The results are listed in Table 2.

For each specimen the cracks (including the irregular helicoidal type) are numbered. The cracks are subdivided into (i) the group of cracks that cannot be classified according to the three main types of fracture topographies (penny-shaped, conoidal and combination of conoidal, and penny-shaped); (ii) the group of cracks that can be classified with an accurate fiber location determination. The results of this classification is shown in Table 3. The dimensions and orientation of the cracks specified geometries are determined with the image analysis procedure. These results are summarized

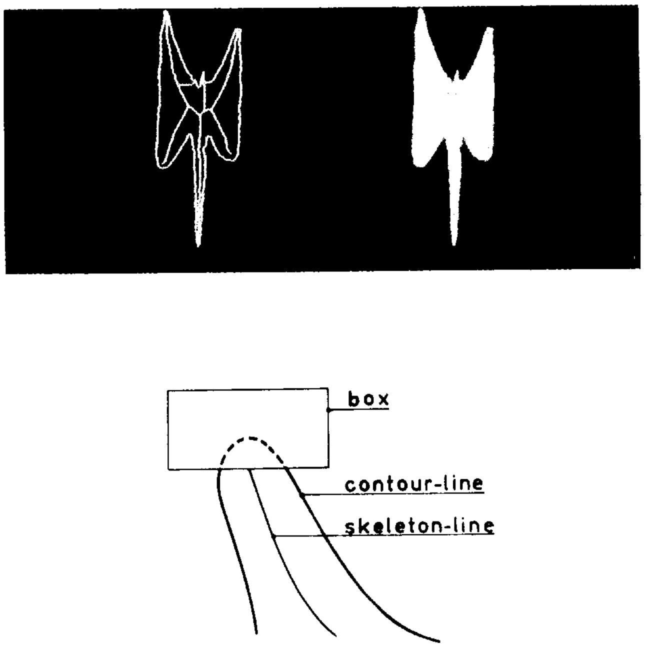

b) Position of removal-box.

Fig. 17 Use of skeletel lines for the isolation of parts of contour

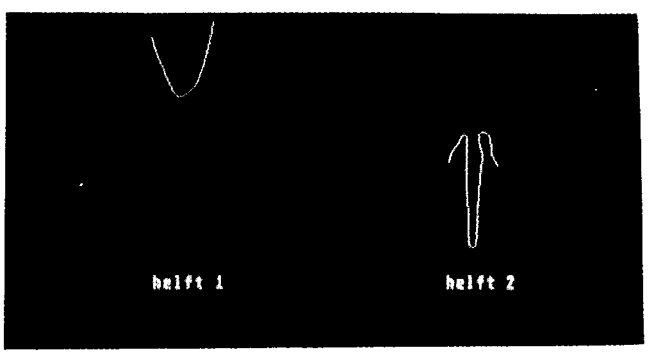

Upper contour. Lower contour.

Fig. 18 Extracted upper and lower contours of matrix crack

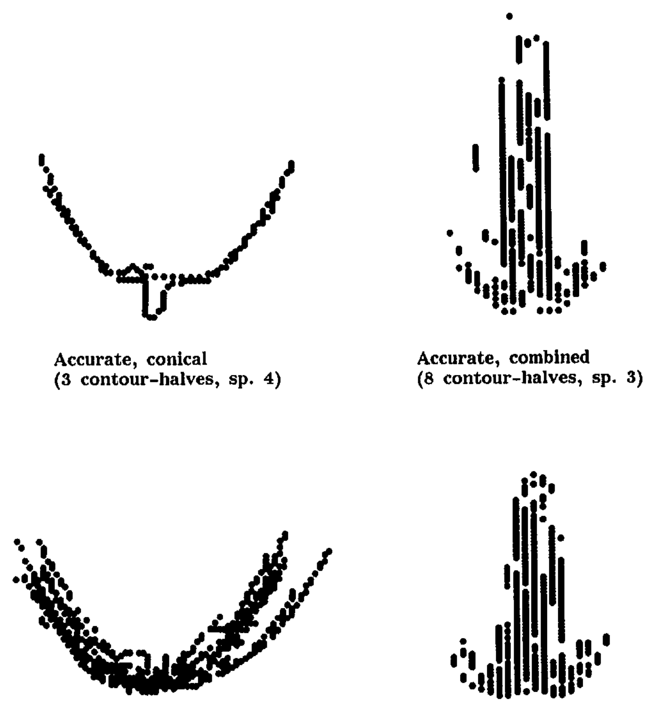

Accurate, conical (3 contour-halves, sp. 4)

Accurate, combined (8 contour-halves, sp. 3)

Approximate, conical (18 contour-halves, sp. 4)

Approximate, combined (11 contour-halves, sp. 3)

Fig. 19 Cumulative image of contour halves (specimens 3 and 4)

Table 3 Distribution of cracks in the tested specimens

Specimen	Number of Cracks			
	Total	Helicoidal (1)	Approximate (2)	Accurate (3)
1	33	21	13	5
2	52	43	5	4
3	46	36	6	4
4	41	16	22	3
5	56	25	26	5

Table 4 Results of crack measurements

Specimen	Number of Crack-Halves	(c/a)	$(c1/a)$	$(c2/a)$	φ_0
Conical (approximate)					
1	12	2.91	-	-	*
2	0	*	-	-	*
3	1	2.05	-	-	57°
4	18	3.19	-	-	45°
5	6	3.18	-	-	45°
Conical (accurate)					
1	6	2.53	-	-	51°
2	3	2.37	-	-	51°
3	0	*	-	-	*
4	3	2.63	-	-	57°
5	1	2.96	-	-	57°
Combined (approximate)					
1	14	-	2.42	3.36	56°
2	10	-	2.78	6.12	63°
3	11	-	1.98	5.63	45°
4	22	-	1.60	4.32	51°
5	46	-	2.44	7.20	56°
Combined (accurate)					
1	4	-	1.69	2.84	56°
2	5	-	1.31	6.53	*
3	8	-	*	*	*
4	3	-	*	*	*
5	9	-	2.17	4.79	56°

(- indicates that the parameter is not applicable; * indicates that no reliable measurement was possible)

in Table 4. In these studies only one isolated penny-shaped crack was observed. Consequently, this category of cracks is not considered further. The results in Table 4 are those for contour-halves, (i.e., one observed crack is divided into two halves and thus yields two contour halves (after image processing).

Conclusions

The engineering properties of a fiber-reinforced composite are strongly influenced by the micromechanical processes that take place within the fibers, the matrix, and at the fiber-matrix interface. The fragmentation tests involving the axial loading of a matrix specimen, containing a single coaxial embedded fiber filament is a possible test for examining the micromechanical processes at the scale of a fiber. In fragmentation tests two phenomena are observed after fiber fracture. When the interface has strength and fracture toughness characteristics that are lower than those of the matrix, fiber ends will experience slip. With the advent of coupling agents, the bond at the fiber-matrix interface can be enhanced with the result that matrix cracking occurs at a cracked fiber location. In this sense the cracked fiber locations act as nuclei for matrix cracking. Fragmentation tests with embedded single-fiber filaments require advanced experimental procedures involving accurate preparation of specimens, their precise uniaxial loading and the development of computer-aided techniques for the evaluation of matrix crack topographies, particularly at cracked fiber locations. This research has developed efficient experimental schemes and computer-aided data evaluation techniques for the study of matrix crack evolution at cracked fiber locations. The experimental studies indicate that at the micromechanical level, stable matrix crack extension can take place at cracked fiber locations. In particular, three major matrix crack propagation patterns are observed. With the aid of the computer-aided image analysis technique, these patterns can be quantified for several levels of longitudinal straining of the fragmentation specimen. The quantification of specific geometrical features of the matrix crack configurations can also be achieved. These include the inclination of the matrix crack at the fiber-matrix interface, the radii of single conoidal cracks and multiple cracks involving conoidal and penny-shaped cracks. The data on crack topographies have been evaluated with a view to examining the efficiency of elementary computational models of crack extension in brittle elastic solids.

The primary motivation for the development and examination of fragmentation tests involving embedded fiber filaments stem from the need to understand micro-mechanical level matrix cracking at cracked fiber locations in fiber-reinforced composites. The methodologies, however, have applications to the study of crack extension at rock anchor regions, anchor bolts in concrete and cracking at the extremities of multiphase composites reinforced with elongated inclusions. The experimental methodologies involving the specimen fabrication and testing are directly applicable to the latter topic. The evaluation of the extent of crack extension can be achieved by ultrasonic and acoustic emission techniques, which can adequately describe the formation of discrete cracks and the precursor microcracks.

Acknowledgments

The authors wish to express their thanks to PPG Industries Fiber Glass bv (Hoogezand, The Netherlands) for supplying specially prepared fibers for the experimentation. The following people from the Laboratory of Engineering Mechanics at Delft University of Technology are thanked for carrying out the experiments: Mr. J. C. Sterk, Miss C. M. van Daalen, and Mr. C. A. J. Toussaint.

References

Atkinson, C., 1979, "Stress Singularities in Fracture Mechanics," ASME *Applied Mechanics Review*, Vol. 32, pp. 123–155.

Berg, R. M., van den, 1990, "Fragmentation Tests with Glass/Polyester and Glass/Epoxy," (in Dutch), Report No. LTM-918 Laboratory of Engineering Mechanics, University of Technology, Delft, The Netherlands.

Busschen, A., ten, 1991, "Micromechanical Modelling of Uni-Directional Glass Fiber Reinforced Polyester: Effect of Matrix Shinkage," *Proc. Euromech Colloquium 269*, A. Vautrin, ed., St. Etienne, France, pp. 1–8.

Chamis, C. C., 1974, "Mechanics of Load Transfer at the Interface," *Interfaces in Polymer Matrix Composites*, Vol. 6, L. J. Broutman and R. H. Crock, eds., Academic Press, New York, pp. 31–77.

Cox, H. L., 1952, "The Elasticity and Strength of Paper and Other Fibrous Materials," *British Jour. Appl. Phys.*, Vol. 3, pp. 72–79.

Dekkers, M. E. J., 1985, "The Deformation Behaviour of Glass Bead Filled Glassy Polymers," Ph.D. Thesis, Tech. Univ. Eindhoven, The Netherlands.

DSM Resins, 1991, *Brochure Synolite*, The Netherlands.

England, A. H., 1965, "A Crack Between Dissimilar Media," ASME Journal of Applied Mechanics, Vol. 32, pp. 400–404.

Friedrich, K., ed., 1989, *Application of Fracture Mechanics to Composite Materials, Composite Materials Series*, Vol. 6, R. B. Pipes, ed., Elsevier, Amsterdam, The Netherlands.

Griffith, A. A., 1921, "The Phenomena of Rupture and Flow in Solids," *Phil. Trans. Roy. Soc. London*, Vol. A221, pp. 163–179.

Hull, D., 1981, *An Introduction to Composite Materials*, Cambridge University Press, Cambridge, U.K.

Kassir, M. K., and Sih, G. C., 1975, *Three Dimensional Crack Problems*, Mechanics of Fracture Series, Vol. 2, G. C. Sih, ed., Noordhoff, Leyden, The Netherlands.

Kedward, K. T., Wilson, R. S., and McLean, S. K., 1989, "Flexure of Simply Curved Composite Shapes," *Composites*, Vol. 20, pp. 527–536.

McCartney, L. N., 1989, "New Theoretical Model of Stress Transfer Between Fibre and Matrix in a Uniaxially Fibre-Reinforced Composite," *Proc. Roy. Soc.*, Vol. A425, pp. 215–244.

Merle, G., and Xie, M., 1991, "Measurement of the Adhesion of Polyester Block Amine to E-Glass by Single Filament Fragmentation," *Composites Science and Technology*, Vol. 40, pp. 19–30.

Moran, B., Gosz, M., and Achenbach, J. D., 1991, "Effect of a Viscoelastic Interfacial Zone on the Mechanical Behaviour and Failure of Fibre-Reinforced Composites," *Proc. IUTAM Symposium*: *Inelastic Deformation of Composite Materials*, G. J. Dvorak, ed., Springer-Verlag, Berlin, pp. 35–49.

Pagano, N. J., ed., 1989, *Interlaminar Response of Composite Materials*, Composite Materials Series, Vol. 3, R. B. Pipes, ed., Elsevier Scientific Publ., Amsterdam.

Pantano, C. G., and Chen, E. J. H., eds., 1990, *Interfaces in Composites*, *Proceedings of the MRS Symposium*, *Boston*, Materials Research Society Symposium Proceedings, Vol. 170, Pittsburgh, PA.

Piggott, M. R., 1980, *Load Bearing Fibre Composites*, Pergamon Press, New York.

Rebelo, C. A. C. C., Ferreira, A. J. M., Marques, A. T., and de Castro, P. M. S. T., 1986, "The Influence of Processing Conditions on Mechanical and Fracture Properties of GRP Plates," *Mechanical Behavior of Composites and Laminates*, W. A. Green and M. Micunovic, eds., Proc. Euromech. Colloquium 214, Kupari, Yugoslavia, Elsevier, Amsterdam, The Netherlands, pp. 54–63.

Sancaktar, E., 1991, "Nonlinear Viscoelastic Behaviour of the Fibre-Matrix Interface, Theory and Experiment," *Proc. Euromech Colloquium* 269, A. Vautrin, ed., St. Etienne, France.

Selvadurai, A. P. S., 1991, "Cracks at the Extremities of Cylindrical Fiber Inclusions," *Proc. IUTAM Symposium on Inelastic Deformation of Composites Materials*, G. J. Dvorak, ed., Springer-Verlag, Berlin, pp. 147–171.

Selvadurai, A. P. S., and Busschen, A. ten, 1995, "Mechanics of a Fragmentation Test Involving an Embedded Fiber, Part II: Computational Modeling and Comparisons," ASME Journal of Applied Mechanics, Vol. 62, pp. 98–107.

Selvadurai, A. P. S., Busschen, A., ten, and Ernst, L. J., 1991, "Batman-Cracks: Observations and Numerical Simulations," *Proc. 13 Can. Congr. Appl. Mech. CANCAM '91*, Winnipeg, Canada, pp. 382–383.

Selvadurai, A. P. S., Singh, B. M., and Au, M. C., 1992, "The Matrix-Fiber Crack in an Elastic Solid," unpublished,

Sih, G. C., and Chen, E. P., 1981, *Cracks in Composite Materials*, *Mechanics of Fracture*, Vol. 6, Martinus Nijhoff, The Hague.

Sneddon, I. N., 1946, "The Stress Distribution in the Neighbourhood of a Crack in an Elastic Solid," *Proc. Roy. Soc.*, *London*, Vol. A187, pp. 229–260.

Toussaint, C. A. J., 1991, "Manual for the Image Analysis Programme TCL," (in Dutch) Report No. LTM 953, Laboratory for Engineering Mechanics, University of Technology, Delft, The Netherlands.

Williams, M. L., 1959, "The Stresses Around a Fault or Crack in Dissimilar Media," *Bulletin Seismological Soc. of America*, Vol. 49, pp. 199–204.